



Electric properties of MnZn ferrite/polyaniline composites: the implication of polyaniline morphology

R. Moučka^{1,*}, N. Kazantseva¹, and I. Sapurina²

¹Centre of Polymer Systems, University Institute, Tomas Bata University in Zlín, Trida T. Bati 5678, 76001 Zlín, Czech Republic

²Institute of Macromolecular Compounds, Russian Academy of Sciences, St. Petersburg, Russia 199004

Received: 10 July 2017

Accepted: 20 September 2017

Published online:

26 September 2017

© Springer Science+Business Media, LLC 2017

ABSTRACT

(Di)electric properties of MnZn ferrite particles coated by conductive (emeraldine salt) and non-conductive (emeraldine base) forms of PANi were measured and discussed in relation to properties of individual components of such composite. The electric response in a wide frequency (0.1 Hz–10 MHz) and temperature (–150 to 100 °C) range was determined. Recorded relaxation processes were identified as a result of hopping charge carriers, which either only polarize or give rise to DC conductivity. Temperature dependence of conductivity modelled by variable range hopping model indicated different system dimensionality: 3D in PANi bulk and 1D in PANi film, that is result of PANi morphology variation. AC conductivity frequency spectra were well approximated by power law model, and temperature evolution of its exponent was related to the type of charge involved in the charge transport. Altogether, the overlayer of conductive PANi increases by two orders of magnitude the electrical conductivity of ferrite/PANi composite compared to pristine ferrite, whereas non-conductive PANi reduced it by three orders of magnitude. Therefore, the electrical properties of ferrite/PANi composites are determined by electrical properties of PANi, which in turn depend upon mesoscale charge transport in PANi.

Introduction

Ferrous oxides (ferrites) have been a subject of scientific research due to their unique combination of magnetic and electric properties. It is the low conductivity, compared to ferromagnetic metals, which makes them an interesting choice for engineering applications where eddy current losses might be an issue [1–5]. Charge transport in ferrites has been

studied mainly in relation to (basic cell) elemental composition and ion's substitution, which may act as doping by decreasing the activation energy of conduction [6]. Despite intensive research in this field, the charge transport mechanism is not fully understood and therefore several explanations are proposed; however, most frequently models on the basis of mobility of activated charge carriers, such as variable range hopping (VRH), are considered.

Address correspondence to E-mail: moucka@cps.utb.cz

Hopping model describes low-temperature conduction in strongly disordered systems with localized charge carrier states [7]. Probability of charge hopping between the states depends on their spatial and energy separation, which in case of purely amorphous systems can be merged into a single range parameter giving probability of the hop between two states. Overall conductivity is then given by the mean nearest-neighbour distance between states as conduction process is seen as many series of hops through these states. The hopping particles are not exclusively electrons but also polarons are registered; more frequently small polarons are observed due to their higher mobility over large polarons [6, 8]. The type of hopping particles involved can be hinted at through temperature dependence of exponent n in Jonscher power law model [9, 10].

Polyaniline (PANi) belongs to the group of well-known conductive polymeric materials, whose conductivity, σ (S cm^{-1}), can be easily controlled by doping level in a wide range [11]. Thus, emeraldine base (EB) of PANi, which is its deprotonated semi-conducting form, has conductivity of about $10^{-8} \text{ S cm}^{-1}$ while protonated emeraldine salt (ES) of PANi can reach conductivity of several S cm^{-1} . Although none of the formulated charge transport mechanisms for PANi have been unanimously accepted, most frequently hopping models are employed to this end [12]. Morphologically PANi can be described by two models: granular 3D metallic islands surrounded by amorphous regions [13, 14] or isolated conducting chains in an insulating matrix [15, 16]. Metallic island model comprises bundles (also referred to as crystalline regions) of coupled chains, in which electrons are completely delocalized. Overall conductivity is then determined by inter-bundle barriers with localized electrons. The measure of disorder describes the localization length α^{-1} [17]. The same applies to the second model where inter-chain interactions dramatically decrease, otherwise much more effective intrachain charge transport. Both models also share the idea of insulator to metal transition which describes percolation between crystalline regions or protonated polymer chains, respectively. One of other convenient features is that PANi readily covers large variety of surfaces immersed into reaction mixture during in situ aniline polymerization [18]. In this way, various “core-shell” particle-based composite materials can be prepared with a number of applications ranging from radio-

absorbing materials (RAMs) [19–22] to magnetically recyclable photocatalyst [23], etc. As regards the use of “core-shell” particles where the core is the magnetic particle and the shell is an electrically conducting polymer (PANi, polypyrrole, etc.) for the design of radio absorbers, their advantage lies in the fact that by changing the thickness and conductivity of the shell it is possible to control the radio frequency dispersion of complex magnetic permeability and permittivity of composites [24, 25].

In the current work, we follow up our previous research devoted to synthesis and properties investigation of MnZn ferrite/PANi [26, 27] and study how PANi overlayer (its protonated and deprotonated form) deposited on the surface of MnZn ferrite particles affects charge transport/DC and AC conductivity of such hybrid core-shell magnetic system. To this end, we employ impedance spectroscopy, which can be used in order to investigate complex phenomena taking place in the system under application of dynamic electric field.

Experimental

Sample preparation

PANi emeraldine salt was synthesized through oxidation of aniline (0.1 M) with ammonium persulfate (0.125 M) in aqueous 0.2 M hydrochloric and sulphuric acid [28]. In addition to electrically conductive PANi-ES, emeraldine base (PANi-EB) was prepared by deprotonation of ES with 1 M NH_4OH .

Ferrite (MnZn) particles of given composition (Table 1) and particle size distribution (from 40 to 80 μm) were coated by in situ polymerization of aniline in hydrochloric and sulphuric as stated in [20, 26, 27]. As a result, ferrite/PANi-ES particles with core-shell structure and PANi content of 6 wt% were obtained. Certain amount of ferrite/PANi-ES particles were deprotonated in order to transform conducting PANi-ES to its nonconducting PANi-EB form (ferrite/PANi-EB).

Dielectric relaxation spectroscopy (DRS)

Dielectric measurements were performed as frequency sweeps (0.1 Hz–10 MHz) in the temperature range from -150 to 80°C with an amplitude of measuring voltage equal to 1 V using impedance

Table 1 Main characteristics of sintered polycrystalline MnZn ferrite used for preparation of micron-sized particles

Sintered MnZn ferrite, 3000-NM (data from manufacturer, Ferroprigor, Russia)	
Fe ₂ O ₃ (mol%)	53.75
MnO (mol%)	25.10
ZnO (mol%)	21.15
Initial magnetic permeability μ_i	2700–3000
Maximum magnetic permeability μ_{max}	3700–5200
Saturation magnetization M_s (kOe)	3.5
Curie temperature T_C (°C)	200
Conductivity σ_f (S cm ⁻¹)	0.0002
Density ρ_f (g cm ⁻³)	4.8
Grain size (μ m)	5–20

analyser (Novocontrol, Germany) on pelletized powder samples in the form of 1-mm-thick discs with diameter of 13 mm. Obtained frequency spectra of complex permittivity ($\epsilon^* = \epsilon' + i\epsilon''$) were transformed into electric modulus M^* :

$$M^* = \frac{1}{\epsilon^*} \tag{1}$$

in order to suppress conductivity contributions, which mask relaxation processes [29]. Temperature dependence of observed relaxation processes was approximated by Arrhenius equation:

$$f_r = f_0 \exp\left(-\frac{W}{kT}\right) \tag{2}$$

where f_r is relaxation frequency, f_0 pre-exponential factor, W activation energy, k Boltzmann constant, and T thermodynamic temperature.

Results and discussion

PANi-ES

Emeraldine salt form of PANi (PANi-ES) is highly conductive as proves the frequency dependence of AC conductivity (Fig. 1), which consists of DC plateau (constant value for measured frequency range indicating DC conductivity) only. Consequently, there are no observable relaxations even in electric modulus (its loss part increases but never reaches a peak in the investigated frequency band). Nevertheless, the charge transport involved can be determined from the temperature dependence of DC conductivity (extracted from DC plateaus). Up to 280 K (then degradation gradually sets in) conductivity is found to increase with temperature following VRH:

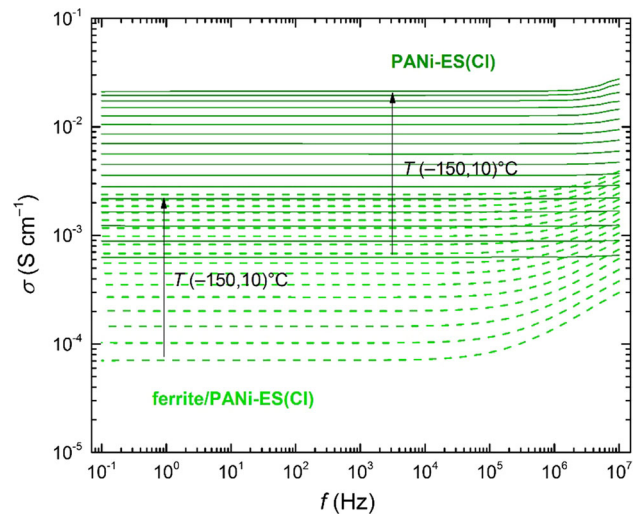


Figure 1 Increase in AC conductivity with temperature (–150 to 10 °C) for samples comprising PANi-ES.

$$\sigma(T) = \sigma_0 \exp\left[-\left(\frac{T_0}{T}\right)^{\frac{1}{D+1}}\right] \tag{3}$$

where D is system dimensionality.

In spite of linear PANi chains ($D = 1$; $R^2 = 0.9975$), better agreement ($R^2 = 0.9994$) is achieved for higher dimensionality, i.e. $D = 3$ (Fig. 2). PANi-ES doped with Cl^- and SO_4^{2-} demonstrates same behaviour.

PANi-EB

In PANi-EB samples prepared by deprotonation from PANi-ES doped by Cl^- and SO_4^{2-} anions two relaxation processes were recorded, seen as ripples of the loss electric modulus surface plot (Fig. 3a). Relaxation process with shorter relaxation time (electric modulus loss peak located at higher frequencies; referred to as primary relaxation) was found to follow Arrhenius temperature dependence ($R^2 = 0.9994$

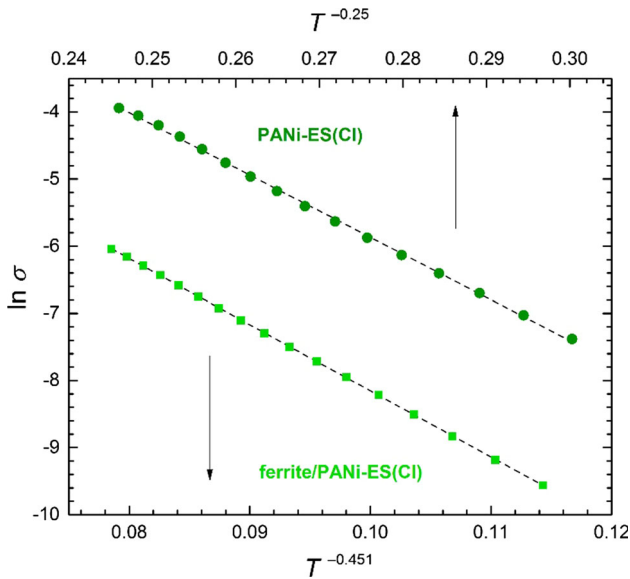


Figure 2 Approximation of conductivity of samples containing PANi-ES by VRH model.

and 0.9996, respectively; Fig. 4) with activation energy (in both samples) equal to 0.53 eV. However, the shape of relaxation peak does not change with temperature, which can be clearly seen from constructing a master curve by normalizing frequency sweeps collected at different temperatures to the point of the peak (Fig. 5). Thus, obtained master curve was well approximated by Havriliak–Negami (HN) model:

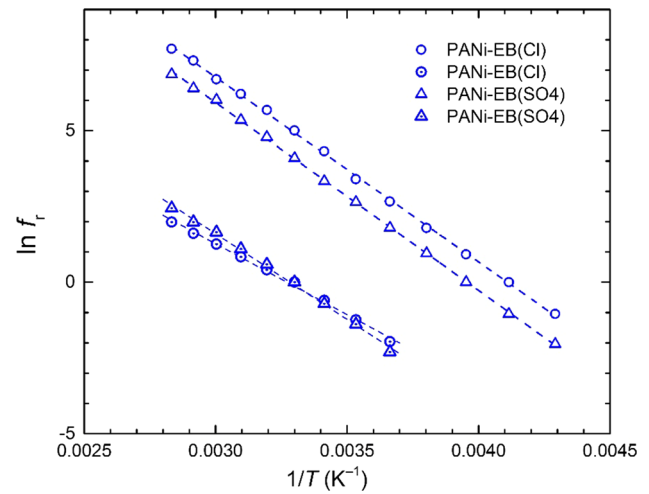


Figure 4 Relaxation map (electric modulus loss peak position) of PANi-EB; primary and secondary peak denoted by empty and dotted symbols, respectively; experimental data approximated by Arrhenius equation.

$$M(\omega)^* = \frac{\Delta M}{[1 + (i\omega\tau)^\beta]^\gamma} \tag{4}$$

Extracted parameters indicate very symmetrical ($\gamma = 0.98$) but rather wide ($\beta = 0.68$) distribution of relaxation times ($\tau = 2.1 \times 10^{-3}$ s; at 20 °C). Activation energy (0.53 eV) value and relaxation time ($\tau = 2.1 \times 10^{-3}$ s; at 20 °C) indicate variable range hopping of charge carriers (electrons/polarons), some of which do remain in the system even after thorough deprotonation. The value of activation

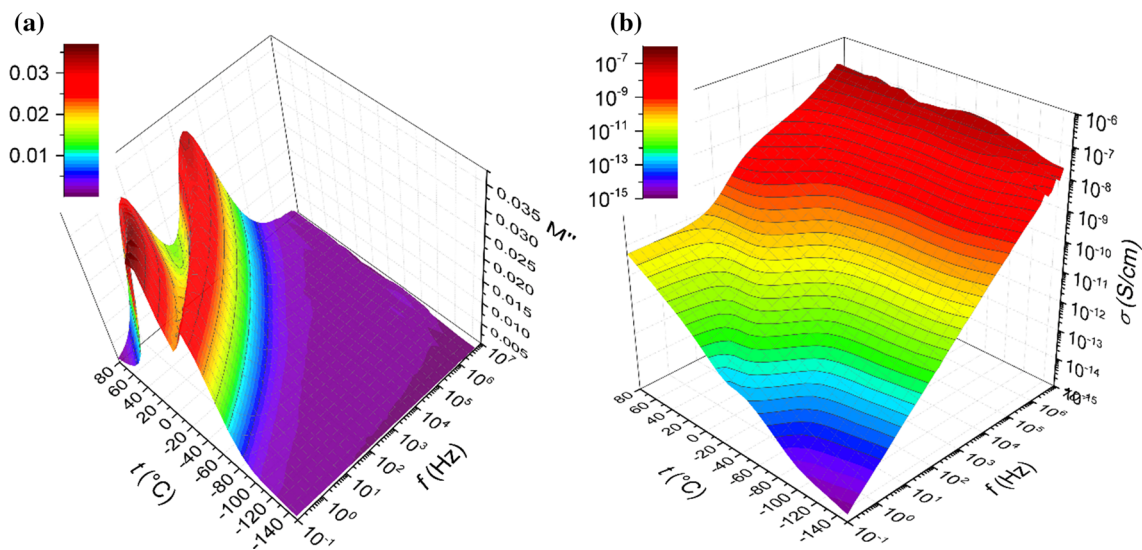


Figure 3 Electric modulus (a) and AC conductivity (b) for PANi-EB (HCl).

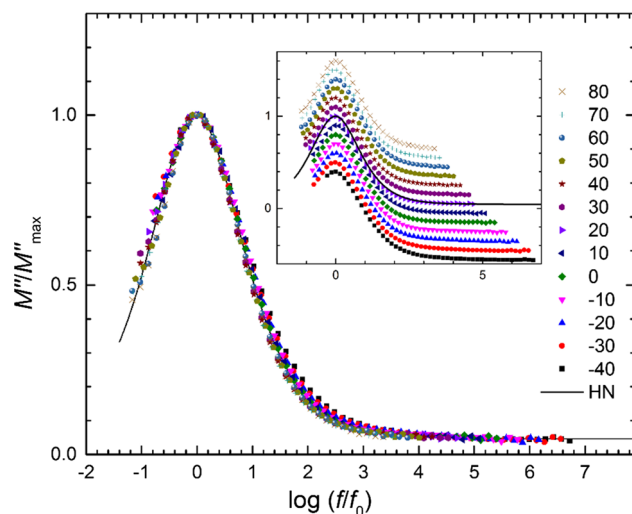


Figure 5 PANi-EB (Cl) relaxation master curve approximated by Havriliak–Negami dielectric model; inset shows individual temperatures vertically shifted.

energy depends on the level to which the sample is deprotonated as well as type of present counter ions (Cl^- and SO_4^{2-}).

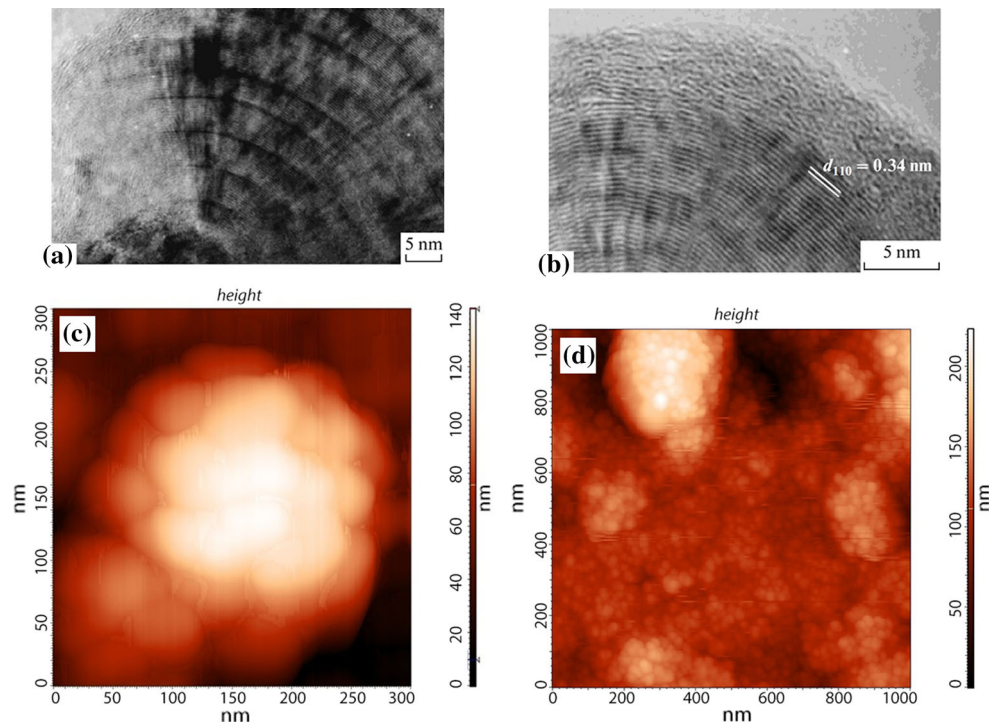
The second process appears at higher temperatures and has longer relaxation times ($\tau = 0.32$ s; at 20 °C; referred to as secondary relaxation) which also change with temperature in agreement with Arrhenius model ($R^2 = 0.997$ for both). Activation energy (W) extracted from loss part of electric modulus equals 0.40 eV (for Cl^-), which rather well matches W of 0.42 eV derived from the temperature shift of the DC conductivity plateau (Fig. 3b). This agreement signifies that the second relaxation process is related to DC conduction of PANi-EB.

The results obtained can be explained from the standpoint of PANi morphology [30]. During polymerization PANi is formed as a large number of individual particles. Under acidic conditions and high concentration of reactants (aniline salt and ammonium persulfate), these particles self-organized into hierarchical formations of different levels [31, 32]. The first level of the hierarchy and the single element from which the whole polymer is “assembled” are the primary spherical particles. These are unimodal particles of a spherical shape, whose diameter, depending on the conditions of synthesis, can vary in the range of tens of nanometres. Polymer spheres consist of crystalline core and amorphous overlayer (Fig. 6a, b). Primary spheres are assembled into quasispherical formations, granules, whose

diameter is hundreds of nanometres (Fig. 6c). Granules represent the second level of hierarchy, which is formed during the stage of polymer chains growth. That is why granules are rather tough, where primary spheres are in a good contact with each other. This is confirmed by the fact that the granules are not broken up either by ultrasound or during the carbonization of PANi at temperatures up to 1000 °C [33]. At the end of the synthesis, during the sedimentation of the insoluble polymer, the granules aggregate and form large agglomerates of irregular shape and size about a micrometre (Fig. 6d). These are particles of the third hierarchical level, where the contact between the granules is weak so such aggregates are easily destroyed.

The correlation between the morphology of PANi and its electrical conductivity was studied by Kelvin probe force and current-sensing atomic-force microscopy [17, 35]. It has been established that the centre of the PANi particles possesses a higher electrical conductivity, whereas on the periphery the conductivity is much lower. Taking into account the aggregation of primary particles into structures with several hierarchical levels, it is possible to explain the ac conductivity within the framework of 3D metallic islands surrounded by amorphous regions. In a macroscopic sample (on a mesoscale), the electrical conductivity is determined by the contacts between particles of different levels of the hierarchy. The central crystalline part of the primary spheres has a high level of electrical conductivity, which is 3D in character. Indeed, in PANi-ES, high electrical conductivity and 3D conductivity character are observed, since the amorphous shell of primary spheres is doped and all particles on the different levels of hierarchy are in good contact. Therefore, PANi-ES exhibits DC conductivity plateau up to 10^6 Hz (Fig. 1). The DC conductivity of macroscopic sample corresponds to the weakest contacts between the particles of the third level of the hierarchy. Deprotonation of PANi-ES affects primarily the amorphous periphery of the primary spheres. Thus, the electrical conductivity of the amorphous overlayer sharply decreases, lowering the contact between the spheres. The presence of DC conductivity plateau on the frequency dependence of PANi-EB AC conductivity is given by the presence of charge carriers in the crystalline part of the primary spheres. Thus, PANi-EB samples demonstrate the presence of two relaxation peaks. The first peak with shorter relaxation time

Figure 6 Hierarchical structure of PANi: **a** and **b** HRTEM images of a polymer sphere, the particle with crystalline core and amorphous shell (first hierarchical level) [34]; **c** AFM images of a granule, i.e. an aggregate of primary spheres (second hierarchical level); **d** agglomerate of granules (third hierarchical level) [31].



($\tau = 2.1 \times 10^{-3} \text{ s}$; at 20°C) apparently indicates relaxation of hopping charges between tightly bonded primary spheres within granules. The second relaxation process with longer relaxation time ($\tau = 0.32 \text{ s}$; at 20°C) is associated with the transport among weakly contacted granules within the micron-sized units. Thus, PANi-EB is very heterogeneous regarding its morphology which is the reason of considerable differences in conductivity: (1) high conductive crystal cores of primary spheres; (2) significantly limited charge transport between the primary spheres through deprotonated amorphous layer; (3) fully depressed transport between granules. As a result, PANi-EB demonstrates dielectric properties.

Ferrite/PANi composites

The electrical conductivity of ferrite/PANi-ES of about $2.6 \times 10^{-3} \text{ S cm}^{-1}$, that is one order lower than for PANi-ES ($2.13 \times 10^{-2} \text{ S cm}^{-1}$), but higher than for pristine ferrite ($5.6 \times 10^{-5} \text{ S cm}^{-1}$). Deprotonation of PANi-ES overlayer results in decrease in conductivity of ferrite/PANi-EB composite up to $4.8 \times 10^{-6} \text{ S cm}^{-1}$, that also is lower than for ferrite but visibly higher than for PANi-EB (10^{-10} to $10^{-8} \text{ S cm}^{-1}$). On the basis of these results and AFM data (Fig. 7), it has been concluded that PANi forms a

continuous layer on the ferrite particles and the conductivity of composite is mostly determined by polymer component. It should be noted that PANi film grown on the ferrite surface does not contain particles of PANi precipitate, i.e. large agglomerates of 1–2 μm in size, third morphological hierarchy of PANi. Therefore, the DC conductivity of ferrite/PANi-EB is determined by the contacts between the polymer spheres in a globule and can be significantly higher than in the PANi-EB.

The temperature dependence of conductivity for ferrite/PANi-ES composite system is described by VRH (Eq. 3). However, the dimensionality of ferrite/PANi-ES is much closer to 1D ($D \sim 1.2$) than that of PANi-ES ($D \sim 2.8$) (Fig. 2). This finding can be explained by different morphology of PANi-ES bulk and PANi-ES film, grown up on ferrite surface.

In the case of in situ deposition method, PANi layer grows directly on the substrate as a result of adsorption onto the surface of initial oligomers [30, 36], i.e. aniline dimers with cyclic structure. For this reason, the nature of the surface influences the morphology and properties of PANi. Preliminary study of in situ growth of PANi layer on the surface of the ferrite showed that the coating of ferrite is not typical and significantly different from the PANi growth, for example, on glass or polystyrene, where a

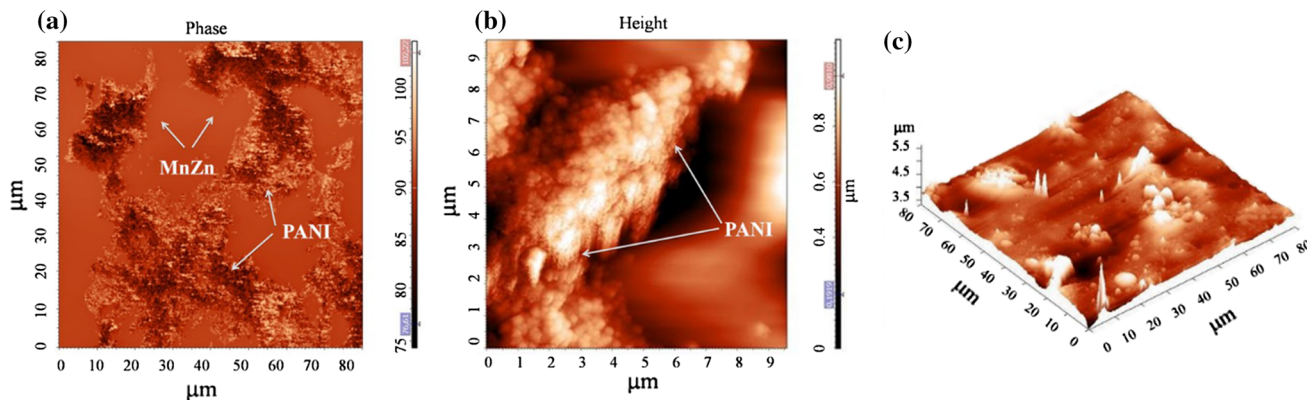


Figure 7 AFM phase images of PANi-ES deposited on the surface of ferrite by in situ polymerization: **a** initial stage of polymerization (discontinuous PANi film with “honeycomb”

structure), **b** PANi “wall”; **c** final stage of polymerization (continuous PANi film with non-uniform thickness, 3D relief) taken from [26, 27].

continuous coating occurs at an early stage of the synthesis. On the ferrite surface, discontinuous PANi film with a “honeycomb” structure forms in the initial stage of polymerization. Polymer grows as walls oriented in different directions, and fixed angles of 90° and 120° between the intersecting walls can be found (Fig. 7a, b) [26]. The size and shape of the cells correspond to the domain structure of ferrite; therefore, we suggest the preferential growth of PANi in outcrops on the domain wall surfaces, where magnetic field is inhomogeneous [26, 27]. The central part of the cell polymer grows only at the final stage of synthesis. The result is a continuous coating, which is non-uniform in the thickness (Fig. 7c). The average thickness of the coating is less than 100 nm. We assume that the change in the nature of charge carrier transport from 3D in the case of PANi-ES to 1D in the case of it ferrite/PANi composite is due to preferential direction of transport along the PANi “walls”, which comprise PANi spheres highly oriented in direction perpendicular to the surface of the ferrite (Fig. 7b).

In order to identify the type of the charge carriers involved in the transport, frequency dependence of conductivity was utilized. Typical AC conductivity plot for ferrite/PANi (Fig. 1) exhibits DC plateau (frequency-independent component) in the whole measured temperature range. DC conductivity increases with temperature, and onset of frequency-dependent component shifts to higher frequencies (resulting in longer DC plateaus). Experimental data are well approximated by Jonscher power law model:

$$\sigma_{AC} = \sigma_{DC} + A\omega^n \tag{5}$$

where σ_{AC} and σ_{DC} are conductivities, A pre-exponential factor, and ω angular frequency.

Temperature dependence of extracted exponent n then indicates involved transport mechanism. Thus, approximation of ferrite/PANi composites’ AC conductivities by Jonscher power law model (Eq. 5) yields monotonously increasing dependence (Fig. 8), which speaks for *small polaron conduction* (SPC) as predominant type of charge transport. However, same dependence for monocrystal ferrite sample exhibits a minimum hinting at *overlapping large polaron tunnelling* (OLPT) [10]. Nevertheless, in the case of ferrite/PANi-EB OLPT cannot be ruled out due to convex shape of the dependence, which can attain a minimum at temperatures below $-150\text{ }^\circ\text{C}$.

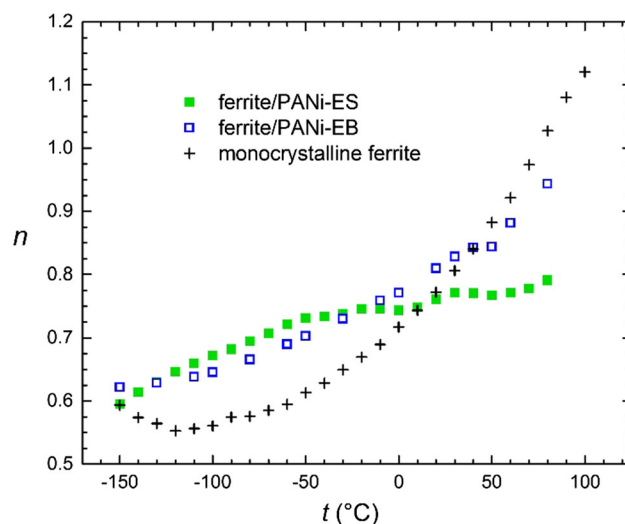


Figure 8 Temperature dependence of Jonscher power law exponent n for ferrite/PANi.

Plotting DC conductivity in Arrhenius plot is able to provide not only comprehensible conductivity comparison of all samples but also an insight into changes in conductivity mechanism with temperature (Fig. 9). In this regard, most pronounced alternation occurs for the least conductive PANi-EB where a temperature-activated conduction takes place. Similar though less pronounced break is recorded for ferrite/PANi-EB where two separate linear regions characterized by constant activation energy can be distinguished (Fig. 10). Assuming small polaron hopping mechanism typical of conduction in ferrite [37]:

$$\sigma = \frac{1}{BT} \exp\left(-\frac{W}{kT}\right) \quad (6)$$

activation energy, W , of the process can be extracted from the slope of $\ln(\sigma T)$ versus $1/T$ dependence (Fig. 10). Abrupt change in the slope indicates an increase in activation energy of conduction process (electron hopping between Fe^{3+} and Fe^{2+}) from 0.12 to 0.26 eV with temperature [38]. Such a break, however, is not present for bulk ferrite, which sees continuous increase in activation energy with temperature. The rest of the investigated systems do not exhibit strong change with temperature.

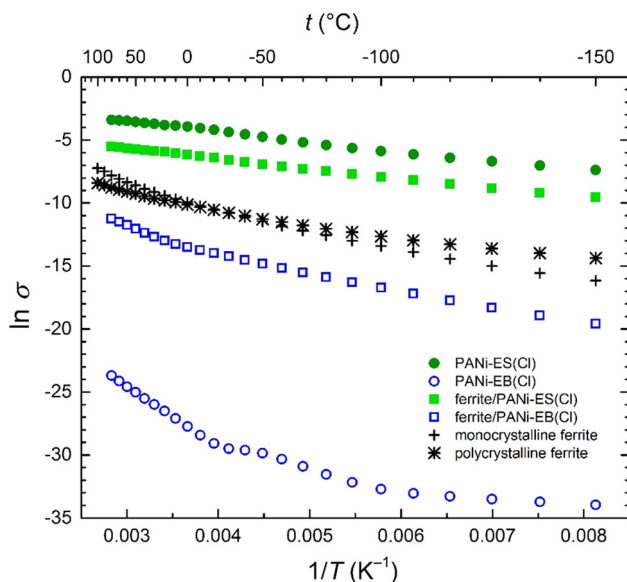


Figure 9 Arrhenius plot (DC conductivity) of PANi, ferrite/PANi composite and ferrite.

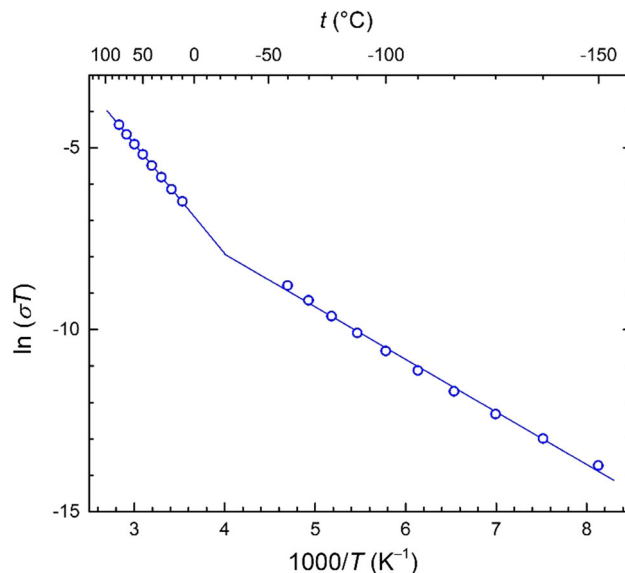


Figure 10 Small polaron hopping model for ferrite/PANi-EB composite exhibiting two regions of different activation energies.

Conclusions

Electric properties of ferrite/PANi composite, comprising ferrite particles coated by PANi, ultimately depend on electric properties of PANi overlayer, which in turn depend upon mesoscale charge transport in PANi, as well as on continuous character of coating. In its conductive form (emeraldine salt), the overlayer can increase conductivity of such composite system while deprotonated PANi (emeraldine base) decreases overall conductivity of ferrite/PANi-EB compared to pristine semiconducting ferrite. Two relaxation processes detected for PANi-EB are connected with the hierarchical structure of the polymer, namely charge (electron) hopping either between primary polymer spheres within the granule or between the granules.

Differences in supramolecular structure of bulk and film PANi-ES shown by microscopy were confirmed by different temperature dependence of DC conductivity; both well approximated by VRH; however, the dimensionality of the transport switches from 3D in PANi-ES bulk to 1D in PANi-ES film. AC conductivity spectra of all samples show DC plateaus and are quantitatively well described by Jonscher power law. The type of hopping charge was estimated from temperature evolution of n exponent in Jonscher power law model. Thus, *overlapping large polaron tunnelling* of ferrite changes after coating with PANi-ES to *small polaron hopping*. Activation energy

of conduction process in ferrite/PANi-EB increases with temperature at two different rates indicating a change in conduction mechanism.

Consequently, it has been shown that PANi coating on top of ferrite particles, used in order to alter magnetic properties of such composite materials [20, 27, 39], can rather significantly change their electric properties.

Acknowledgements

This work was supported by the Ministry of Education, Youth and Sports of the Czech Republic—Program NPU I [LO1504].

References

- [1] Kong LB, Li ZW, Liu L, Huang R, Abshinova M, Yang ZH et al (2013) Recent progress in some composite materials and structures for specific electromagnetic applications. *Int Mater Rev* 58:203–259
- [2] Li BW, Shen Y, Yue ZX, Nan CW (2006) Enhanced microwave absorption in nickel/hexagonal-ferrite/polymer composites. *Appl Phys Lett* 89:132504
- [3] Yusoff AN, Abdullah MH, Ahmad SH, Jusoh SF, Mansor AA, Hamid SAA (2002) Electromagnetic and absorption properties of some microwave absorbers. *J Appl Phys* 92:876–882
- [4] Kazantsev YN, Lopatin AV, Kazantseva NE, Shatrov AD, Mal'tsev VP, Vilcakova J et al (2010) Broadening of operating frequency band of magnetic-type radio absorbers by FSS incorporation. *IEEE Trans Antennas Propag* 58:1227–1235
- [5] Bespyatykh YI, Kazantseva NE (2008) Electromagnetic properties of hybrid polymer composites. *J Commun Technol Electron* 53:143–154
- [6] Fukuda Y, Nagata S, Echizenya K (2004) Electrical conductivity of MnZn ferrite single crystals with a small number of Fe²⁺ ions. *J Magn Magn Mater* 279:325–330
- [7] Mott NF (1969) Conduction in non-crystalline materials.3. Localized states in a pseudogap and near extremities of conduction and valence bands. *Philos Mag* 19:835–852
- [8] Walz F (2002) The Verwey transition—a topical review. *J Phys-Condens Mater* 14:R285–R340
- [9] Ortega N, Kumar A, Bhattacharya P, Majumder SB, Katiyar RS (2008) Impedance spectroscopy of multiferroic PbZr_xTi_{1-x}O₃/CoFe₂O₄ layered thin films. *Phys Rev B* 77:014111
- [10] Panda RK, Muduli R, Kar SK, Behera D (2014) Dielectric relaxation and conduction mechanism of cobalt ferrite nanoparticles. *J Alloy Compd* 615:899–905
- [11] Bhadra S, Khastgir D, Singha NK, Lee JH (2009) Progress in preparation, processing and applications of polyaniline. *Prog Polym Sci* 34:783–810
- [12] Gosh M, Barman A, Meikap AK, De SK, Chatterjee S (1999) Hopping transport in HCl doped conducting polyaniline. *Phys Lett A* 260:138–148
- [13] Wang ZH, Scherr EM, Macdiarmid AG, Epstein AJ (1992) Transport and EPR studies of polyaniline—a quasi-one-dimensional conductor with 3-dimensional metallic states. *Phys Rev B* 45:4190–4202
- [14] Wang ZH, Ray A, Macdiarmid AG, Epstein AJ (1991) Electron localization and charge transport in poly(o-toluidine)—a model polyaniline derivative. *Phys Rev B* 43:4373–4384
- [15] Mizoguchi K, Nechtschein M, Travers JP, Menardo C (1989) Spin dynamics in the conducting polymer, polyaniline. *Phys Rev Lett* 63:66–69
- [16] Nechtschein M, Genoud F, Menardo C, Mizoguchi K, Travers JP, Villeret B (1989) On the nature of the conducting state of polyaniline. *Synth Met* 29:E211–E218
- [17] Kahol PK, Perera RP, Kumar KKS, Geetha S, Trivedi DC (2003) Electron localization length in polyaniline. *Solid State Commun* 125:369–372
- [18] Maia DJ, De Paoli MA, Alves OL, Zarbin AJG, das Neves S (2000) Conductive polymer synthesis in solid host matrices. *Quim Nova* 23:204–215
- [19] Xu P, Han XJ, Wang C, Zhou DH, Lv ZS, Wen AH et al (2008) Synthesis of electromagnetic functionalized nickel/polypyrrole core/shell composites. *J Phys Chem B* 112:10443–10448
- [20] Kazantseva NE, Vilcakova J, Kresalek V, Saha P, Sapurina I, Stejskal J (2004) Magnetic behaviour of composites containing polyaniline-coated manganese-zinc ferrite. *J Magn Magn Mater* 269:30–37
- [21] Saini P, Choudhary V, Vijayan N, Kotnala RK (2012) Improved electromagnetic interference shielding response of poly(aniline)-coated fabrics containing dielectric and magnetic nanoparticles. *J Phys Chem C* 116:13403–13412
- [22] Makeiff DA, Huber T (2006) Microwave absorption by polyaniline-carbon nanotube composites. *Synth Met* 156:497–505
- [23] Xiong P, Chen Q, He MY, Sun XQ, Wang X (2012) Cobalt ferrite-polyaniline heteroarchitecture: a magnetically recyclable photocatalyst with highly enhanced performances. *J Mater Chem* 22:17485–17493
- [24] Babayan V, Kazantseva NE, Sapurina I, Moucka R, Stejskal J, Saha P (2013) Increasing the high-frequency magnetic

- permeability of MnZn ferrite in polyaniline composites by incorporating silver. *J Magn Magn Mater* 333:30–38
- [25] Kazantseva NE (2012) Magnetic particle-filled polymer microcomposites. *Polymer composites*. Wiley, Weinheim, pp 613–672
- [26] Babayan V, Kazantseva NE, Moucka R, Sapurina I, Spivak YM, Moshnikov VA (2012) Combined effect of demagnetizing field and induced magnetic anisotropy on the magnetic properties of manganese-zinc ferrite composites. *J Magn Magn Mater* 324:161–172
- [27] Babayana V, Kazantseva NE, Sapurina I, Moucka R, Vilcakova J, Stejskal J (2012) Magnetoactive feature of in situ polymerised polyaniline film developed on the surface of manganese–zinc ferrite. *Appl Surf Sci* 258:7707–7716
- [28] Stejskal J, Sapurina I, Trchova M, Konyushenko EN (2008) Oxidation of aniline: polyaniline granules, nanotubes, and oligoaniline microspheres. *Macromolecules* 41:3530–3536
- [29] Gerhardt R (1994) Impedance and dielectric-spectroscopy revisited - distinguishing localized relaxation from long-range conductivity. *J Phys Chem Solids* 55:1491–1506
- [30] Sapurina I, Shishov MA (2012) Oxidative polymerization of aniline: molecular synthesis of polyaniline and the formation of supramolecular structures. In: Gomes ADS (ed) *New polymers for special applications*. InTech, Rijeka
- [31] Shishov MA, Moshnikov VA, Sapurina IY (2013) Self-organization of polyaniline during oxidative polymerization: formation of granular structure. *Chem Pap* 67:909–918
- [32] Wessling B (2001) From conductive polymers to organic metals. *Chem Innov* 31:34
- [33] Rozlívková Z, Trchová M, Exnerová M, Stejskal J (2011) The carbonization of granular polyaniline to produce nitrogen-containing carbon. *Synth Met* 161:1122–1129
- [34] Mazerolles L, Folch S, Colomban P (1999) Study of polyanilines by high-resolution electron microscopy. *Macromolecules* 32:8504–8508
- [35] O’Neil KD, Shaw B, Semenikhin OA (2007) On the origin of mesoscopic inhomogeneity of conducting polymers. *J Phys Chem B* 111:9253–9269
- [36] Sapurina I, Tenkovtsev AV, Stejskal J (2015) Conjugated polyaniline as a result of the benzidine rearrangement. *Polym Int* 64:453–465
- [37] Mahjoub S, Baazaoui M, M’Nassri R, Boudjada NC, Oumezzine M (2015) Electrical conduction and percolation model in $\text{Pr}_{0.6}\text{Ca}_{0.1}\text{Sr}_{0.3}\text{Mn}_{1-x}\text{Fe}_x\text{O}_3$ ($x = 0, 0.05, \text{ and } 0.075$) manganites. *J Supercond Novel Magn* 28:1905–1911
- [38] Idrees M, Nadeem M, Hassan MM (2010) Investigation of conduction and relaxation phenomena in $\text{LaFe}_{0.9}\text{Ni}_{0.1}\text{O}_3$ by impedance spectroscopy. *J Phys D Appl Phys* 43:155401
- [39] Kazantseva NE, Bespyatykh YI, Sapurina I, Stejskal J, Vilcakova J, Saha P (2006) Magnetic materials based on manganese-zinc ferrite with surface-organized polyaniline coating. *J Magn Magn Mater* 301:155–165